Biophysical Chemistry 23 (1985) 1–13
Elsevier

BPC 01020

DYNAMIC LIGHT SCATTERING FROM DILUTE SUSPENSIONS OF THIN DISCS AND THIN RODS AS LIMITING FORMS OF CYLINDER, ELLIPSOID AND ELLIPSOIDAL SHELL OF REVOLUTION

Satoru FUJIME [a] and Kenji KUBOTA [b]

[a] *Mitsubishi-Kasei Institute of Life Sciences, Machida, Tokyo 194, and* [b] *Department of Physics, Ochanomizu University, Bunkyo-ku, Tokyo 112, Japan*

Received 23rd April 1985
Revised manuscript received 28th May 1985
Accepted 15th June 1985

Key words: Dynamic light scattering; Anisotropic translational diffusion; Rotational diffusion; Rod; Disc

A previous formulation of the field correlation function $G^1(\tau)$ of light quasielastically scattered from suspensions of rigid rods undergoing anisotropic translational as well as rotational diffusion (T. Maeda and S. Fujime, Macromolecules 17 (1984) 1157) was extended to the cases of suspensions of cylinders (length L and radius R), ellipsoids and ellipsoidal shells of revolution ($x^2/b^2 + y^2/b^2 + z^2/a^2 = 1$). The present formulation includes that for suspensions of rigid rods in the limit of $KR \ll 1$ or in the limit of $b/a \ll 1$ and $Kb \ll 1$ (an extremely prolate ellipsoid), and also that for suspensions of discs in the limit of $KL \ll 1$ or in the limit of $b/a \gg 1$ and $Ka \ll 1$ (an extremely oblate ellipsoid), where K is the length of the scattering vector. Explicit forms of $G^1(\tau)$, of the first cumulant $\bar{\Gamma}$ of $G^1(\tau)$ and of the dynamic form factors will be given, and numerical methods suitable for computation of dynamic form factors will be discussed. The present results can be applied to the analysis of experimental data for dilute suspensions of thin rods and thin discs. When the situation is favorable, our method can provide transport coefficients D_1, D_3 and Θ from dynamic light-scattering data only, where D_1 and D_3 are, respectively, the translational diffusion coefficients parallel with the x (y) and z axes, and Θ the rotational diffusion coefficient around the x (y) axis.

1. Introduction

Dynamic light scattering is a powerful tool for studying the dynamics of bio-macromolecules and organelles. Fundamentals of both theoretical and experimental aspects of this technique will be found in standard textbooks [1,2], and extensive application in recent monographs [3–5]. To the best of our knowledge, however, there are no reports up to now on theoretical and experimental studies of dynamic light scattering from suspensions of discs. By a disc, we mean a circular plate whose radius is much larger than its thickness. In this paper, therefore, we will present a theoretical basis for the spectrum of light quasielastically scattered from suspensions of rigid discs.

First, we will consider light scattering from a suspension of cylindrical bodies of radius R and length L. Then, the result can be reduced to that for a rigid rod when $KR \ll 1$ and that for a rigid disc when $KL \ll 1$, where K is the length of the scattering vector $\boldsymbol{K}$. Although the formulation for rigid rods has been presented [6], we again discuss briefly the theoretical result for rigid rods in order to clarify the differences and similarities between spectra for rigid rods and rigid discs.

In the appendices, numerical methods suitable for computation of dynamic form factors will be given, and theoretical expressions for dynamic light-scattering spectra for suspensions of ellipsoids and ellipsoidal shells of revolution will be discussed in connection with the results for discs and rods.

In the accompanying paper [7], we will give

experimental results on suspensions of purple membranes prepared from *Halobacterium halobium*, where the present formulation will be applied to an analysis of experimental spectra.

2. Model

Let us consider a smooth cylinder (length L and diameter $2R$), in which the mass distribution is uniform (fig. 1a). The position vector $\boldsymbol{r}(t)$ of a volume element $\mathrm{d}v$ in the cylinder at time t is given by $\boldsymbol{r}(t) = \boldsymbol{R}(t) + \boldsymbol{j}(t)$, where $\boldsymbol{R}(t)$ is the position vector of the center-of-mass of the cylinder in the laboratory-fixed coordinate system $[X, Y, Z]$ and $\boldsymbol{j}(t)$ that of the volume element of which cylindrical coordinates in the molecule-fixed coordinate system (x, y, z) are given by $(\rho \cos\phi, \rho \sin\phi, z)$. The amplitude of light scattered from the cylinder in fig. 1 is proportional to

$$a(K, \theta, t) = \exp[i\boldsymbol{K}\cdot\boldsymbol{R}(t)] \times (1/\pi R^2 L)\iiint \exp[i\boldsymbol{K}\cdot\boldsymbol{j}(t)]\,\mathrm{d}v$$

This integration can easily be performed in the molecule-fixed coordinate system: Let θ, Φ and Ψ be the Eulerian angles (fig. 1b). Then, we have $\boldsymbol{K} = [0, 0, K] = (-K\cos\Phi\sin\theta, K\sin\Phi\sin\theta, K\cos\theta)$ and $\boldsymbol{K}\cdot\boldsymbol{j} = K\rho\cos(\Phi+\phi)\sin\theta + Kz\cos\theta$, i.e. integration over $\rho\,\mathrm{d}\rho\,\mathrm{d}\phi\,\mathrm{d}z$ gives

$$a(K, \xi, t) = \exp[i\boldsymbol{K}\cdot\boldsymbol{R}(t)] \times [2J_1(Y)/Y] \times j_0(k\xi)$$

where $J_1(z)$ is the first-order Bessel function, $j_0(z) = (\sin z)/z$ the zeroth-order spherical Bessel function, $\xi = \cos\theta$, $k = KL/2$ and $Y = KR\sin\theta = X(1-\xi^2)^{1/2}$ with $X = KR$. As expected for a uniform cylinder, the amplitude $a(K, \xi, t)$ depends on angle θ but not on angles Φ and Ψ, i.e., no effect on $a(K, \xi, t)$ of rotation of the cylinder around its z-axis and around the Z-axis keeping θ unchanged.

The unnormalized field correlation function of polarized scattered light is given by $G^1(\tau) = \langle a(K, \xi, t)a(-K, \xi', t')\rangle$, where $\tau = |t - t'|$ and $\langle \ldots \rangle$ indicates the statistical average. From our previous result [6], we have

$$G^1(\tau) = G_D(\tau) \times \tfrac{1}{2}\int\int_{-1}^{1} [2J_1(Y)/Y] \times [2J_1(Y')/Y']\, j_0(k\xi)\, j_0(k\xi') \times g_K(\xi, \xi'; \tau)\,\mathrm{d}\xi\,\mathrm{d}\xi' \qquad (1)$$

where

$$G_D(\tau) = \exp\left[-\left\{D_0 - \tfrac{1}{3}(D_3 - D_1)\right\}K^2\tau\right] = \exp(-D_1K^2\tau)$$

and $g_K(\xi, \xi'; \tau)$ satisfies the following diffusion equation

$$\left[\partial/\partial\tau - \Theta\left(\nabla_\xi^2 - \mu^2\xi^2\right)\right] g_K(\xi, \xi'; \tau) = \delta(\xi - \xi')\delta(\tau) \qquad (2)$$

where D_1 and D_3 are translational diffusion coefficients along the $x(y)$ and z axes of the cylinder, respectively, $D_0 = (2D_1 + D_3)/3$ the overall translational diffusion coefficient, Θ the end-over-end rotational diffusion coefficient, $\mu^2 = (D_3 - D_1)K^2/\Theta$ the coupling constant between translational and rotational diffusive motions and $\nabla_\xi^2 = (\partial/\partial\xi)(1-\xi^2)(\partial/\partial\xi)$ the Laplace operator. By following the previous procedure [6], eq. 2 can easily be solved: By expanding $g_K(\xi, \xi'; \tau)$ in

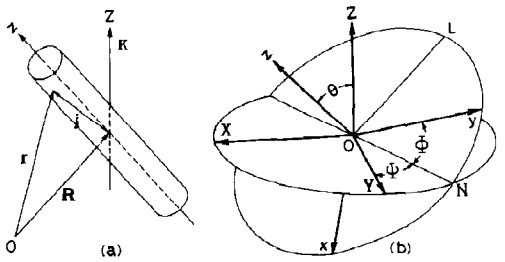

Fig. 1. Geometrical relationship. (a) A vectorial relationship which defines the position vector $\boldsymbol{r}$ of the volume element $\mathrm{d}v$ in a cylinder. $\boldsymbol{R}$ is the position vector of the center-of-mass of, and $\boldsymbol{j}$ the position vector of $\mathrm{d}v$ relative to the center of, the cylinder. The cylinder axis is denoted by z, and the laboratory-fixed axis parallel with the scattering vector $\boldsymbol{K}$ by Z. (b) The Eulerian angles (θ, Φ, Ψ) which define the relative orientation between the laboratory-fixed coordinates $[X, Y, Z]$ and the molecule-fixed coordinates (x, y, z). The line ON shows the intersection between the $[X, Y]$ and (x, y) planes, and the line OL is perpendicular to the line ON.

terms of the Legendre polynomial $P_n(\xi)$, substituting it into eq. 2, multiplying both sides by $P_n(\xi)$, and integrating over ξ, we have simultaneous first-order differential equations for the expansion coefficients $A_n(K, \xi', \tau)$, which can be written in a matrix form as

$$\partial \boldsymbol{A}/\partial\tau = -\Theta \boldsymbol{M}\boldsymbol{A} \tag{3}$$

where $\boldsymbol{A} = [A_0, A_2, \ldots, A_N]^{\mathrm{T}}$ (T signifies transposition, A_n was truncated at $n = N$ and A_n for odd n is not required as shown later) and $\boldsymbol{M} = \{a_{m,n}\}$ with $a_{n,n} = n(n+1) + \mu^2 L_0(n)$, $a_{n,n-2} = \mu^2 L_1(n)$, $a_{n,n+2} = \mu^2 L_2(n)$ and other $a_{m,n}$ elements are all zero. $L_i(n)$ are given by

$$\begin{aligned} L_0(n) &= (2n^2 + 2n - 1)/(2n-1)/(2n+3) \\ L_1(n) &= n(n+1)/(2n-1)/(2n-3) \\ L_2(n) &= (n+1)(n+2)/(2n+3)/(2n+5) \end{aligned} \tag{4}$$

By using a matrix $\boldsymbol{U}$ which satisfies $\boldsymbol{M}\boldsymbol{U} = \boldsymbol{U}\boldsymbol{\Lambda}$, where $\boldsymbol{\Lambda}$ is a diagonal matrix, we have the solution of eq. 3 as

$$\boldsymbol{A}(\tau) = \left[\boldsymbol{U}\exp(-\Theta\boldsymbol{\Lambda}\tau)\boldsymbol{U}^{-1}\right]\boldsymbol{A}(0)$$

with the initial value $A_n(K, \xi', 0) = [(2n+1)/2]P_n(\xi')$. Then, we have

$$\begin{aligned} g_{\mathrm{K}}(\xi, \xi'; \tau) &= \sum_n \sum_l \frac{2l+1}{2} \\ &\quad \times \left[\boldsymbol{U}\exp(-\Theta\boldsymbol{\Lambda}\tau)\boldsymbol{U}^{-1}\right]_{nl} P_n(\xi) P_l(\xi') \end{aligned} \tag{5}$$

From eqs. 1 and 5, $G^1(\tau)$ can be written as

$$\begin{aligned} G^1(\tau) &= G_{\mathrm{D}}(\tau) \sum_n \sum_l (2l+1) \\ &\quad \times \left[\boldsymbol{U}\exp(-\Theta\boldsymbol{\Lambda}\tau)\boldsymbol{U}^{-1}\right]_{nl} \\ &\quad \times c_n(X, k) c_l(X, k) \end{aligned} \tag{6}$$

$$= \sum_p P_p(X, k) \exp(-\Gamma_p \tau) \tag{6'}$$

where

$$\begin{aligned} c_n(X, k) &= \int_0^1 \left[2J_1(Y)/Y\right] j_0(k\xi) P_n(\xi) \mathrm{d}\xi \quad \text{(even } n\text{)} \\ &= 0 \quad \text{(odd } n\text{)} \end{aligned} \tag{7}$$

$$\begin{aligned} P_p(X, k) &= \sum_n \sum_l (2l+1) U_p(n) U_p^*(l) \\ &\quad \times c_n(X, k) c_l(X, k) \end{aligned} \tag{8}$$

$$\Gamma_p = \left[D_0 - \tfrac{1}{3}(D_3 - D_1)\right] K^2 + \lambda_p \Theta \tag{9}$$

$U_p(n)$ is the (n, p) element of $\boldsymbol{U}$, $U_p^*(l)$ the (p, l) element of $\boldsymbol{U}^{-1}$ and λ_p the (p, p) element of $\boldsymbol{\Lambda}$.

To obtain $\boldsymbol{U}$ and $\boldsymbol{\Lambda}$, machine computation is generally useful. In some cases, however, perturbation calculation is applicable. The first-order perturbation results for $U_p(n)$ and $U_p^*(l)$ give [6]

$$\begin{aligned} P_p(X, k) &= (2p+1) c_p(X, k) \Big[c_p(X, k) \\ &\quad + 2\mu^2 L_2(p-2) \\ &\quad \times c_{p-2}(X, k)/(\lambda_p^\circ - \lambda_{p-2}^\circ) \\ &\quad - 2\mu^2 L_1(p+2) \\ &\quad \times c_{p+2}(X, k)/(\lambda_{p+2}^\circ - \lambda_p^\circ) \Big] \end{aligned} \tag{8'}$$

where $\lambda_p^\circ = p(p+1) + \mu^2 L_0(p)$ is the (p, p) element of $\boldsymbol{M}$. The second-order perturbation result for λ_p gives [8]

$$\begin{aligned} \Gamma_p &= \left[D_0 - \tfrac{1}{3}(D_3 - D_1)\right] K^2 + p(p+1)\Theta \\ &\quad + (D_3 - D_1) K^2 L_0(p) \\ &\quad + \left[A_{p-2}(\mu^2) - A_p(\mu^2)\right] \left[(D_3 - D_1)^2/\Theta\right] K^4 \end{aligned} \tag{9'}$$

The explicit form of $A_p(\mu^2)$ is given in ref. 8.

Using the relationship $\bar{\Gamma} = -(\partial/\partial\tau)\ln G^1(\tau)|_{\tau=0}$, we have from eq. 6

$$\begin{aligned} \bar{\Gamma}/K^2 &= \left[D_0 - \tfrac{1}{3}(D_3 - D_1)\right] \\ &\quad + (1/K^2) \sum_n \sum_l (2l+1) \boldsymbol{M}_{nl} \\ &\quad \times c_n(X, k) c_l(X, k)/G^1(0) \\ &= \left[D_0 - \tfrac{1}{3}(D_3 - D_1)\right] + \langle R_{\mathrm{g}}^2 \rangle \Theta h_1(X, k) \\ &\quad + (D_3 - D_1) h_2(X, k) \end{aligned} \tag{10}$$

where $\langle R_{\mathrm{g}}^2 \rangle$ is the mean-square radius of gyration around the x-axis in fig. 1 and $G^1(0) = \Sigma_n (2n+1) c_n(X, k)^2$. Since $\boldsymbol{M}_{nl}$ is the (n, l) element of

$M, h_1(X, k)$ and $h_2(X, k)$ are given by

$$h_1(X, k) = \frac{1}{\langle R_g^2 \rangle K^2} \sum_n n(n+1)(2n+1) \times c_n(X, k)^2 / G^1(0) \quad (11)$$

$$h_2(X, k) = \sum_n (2n+1) c_n(X, k) [L_0(n) c_n(X, k) + L_2(n-2) c_{n-2}(X, k) + L_1(n+2) c_{n+2}(X, k)] / G^1(0) \quad (12)$$

where $(2n-3)L_1(n) = (2n+1)L_2(n-2)$ and $(2n+5)L_2(n) = (2n+1)L_1(n+2)$ were used.

The numerical computation of $c_n(X, k)$ is not difficult. When both X and k are not small, however, the so-called Rayleigh-Debye condition is not fulfilled and the present expressions have only qualitative meanings [6]. Furthermore, $c_n(X, k)$ has two parameters. Therefore, we consider only two limiting cases, $X \ll 1$ (rod) and $k \ll 1$ (disc).

2.1. Thin rods

In this case, $X = KR \ll 1$ and $2J_1(Y)/Y \simeq 1$. Then, we have

$$c_n(0, k) = \int_0^1 j_0(k\xi) P_n(\xi) \mathrm{d}\xi = (i)^n b_n(k) \quad (\text{even } n) \quad (13)$$

From eq. 10, we have

$$\bar{\Gamma}/K^2 = [D_0 - \tfrac{1}{3}(D_3 - D_1)] + (L^2/12)\Theta f_1(k) + (D_3 - D_1) f_2(k) \quad (14)$$

where $f_1(k) \equiv h_1(0, k)$ and $f_2(k) \equiv h_2(0, k)$;

$$f_1(k) = (3/k^2) \sum_n n(n+1)(2n+1) b_n(k)^2 / G^1(0) \quad (15)$$

$$f_2(k) = \sum_n (2n+1) b_n(k) [L_0(n) b_n(k) - L_2(n-2) b_{n-2}(k) - L_1(n+2) b_{n+2}(k)] / G^1(0) \quad (16)$$

Numerical computation of $b_n(k)$, $f_1(k)$ and $f_2(k)$ is so easy (see appendices A and B) that numerical results are shown graphically only for later comparison; $b_n(k)$ in fig. 2, and $f_1(k)$ and $f_2(k)$ in fig. 3. Eqs. 6 and 14 have been successfully applied to the analysis of experimental data for dilute solutions of tobacco mosaic virus [8].

2.2. Thin discs

Since $k = KL/2 \ll 1$ and $j_0(k\xi) \simeq 1$, eq. 7 gives

$$a_n(X) \equiv c_n(X, 0) = 2 \int_0^1 [J_1(Y)/Y] P_n(\xi) \mathrm{d}\xi \quad (\text{even } n) \quad (17)$$

The factor $a_0(X)$ can be calculated analytically;

$$a_0(X) = (2/X) \int_0^{\pi/2} J_1(X \sin\theta) \mathrm{d}\theta = \sin^2(X/2)/(X/2)^2 \quad (18)$$

from which we know $a_0(X) = 0$ for $X = 2\pi m$ where m is any positive integer. Then, up to the first order in μ^2, eq. 8′ gives $P_0(X, 0) = 0$ for $X = 2\pi m$. Eq. 10 gives

$$\bar{\Gamma}/K^2 = [D_0 - \tfrac{1}{3}(D_3 - D_1)] + (R^2/4)\Theta g_1(X) + (D_3 - D_1) g_2(X) \quad (19)$$

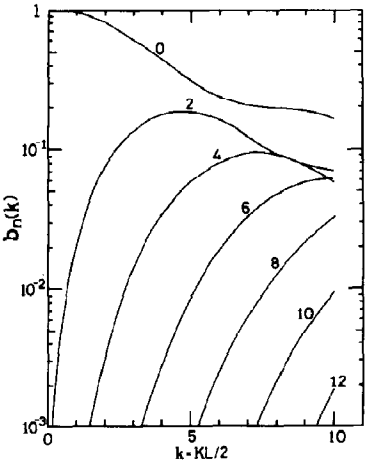

Fig. 2. Graphic representation of the dynamic form factors $b_n(k)$ for a rigid rod with length L.

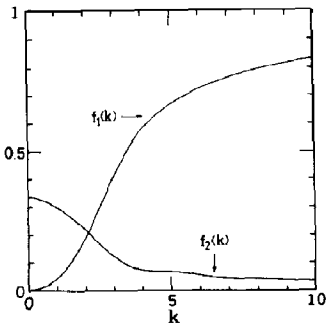

Fig. 3. Graphic representation of the functions $f_1(k)$ and $f_2(k)$ for a rigid rod. Note a slight shoulder in $f_2(k)$ at around $k = 5$.

where $g_1(X) \equiv h_1(X, 0)$ and $g_2(X) \equiv h_2(X, 0)$;

$$g_1(X) = (2/X)^2 \sum_n n(n+1)(2n+1) \times a_n(X)^2 / G^1(0) \quad (20)$$

$$g_2(X) = \sum_n (2n+1) a_n(X) \left[L_0(n) a_n(X) + L_2(n-2) a_{n-2}(X) + L_1(n+2) a_{n+2}(X) \right] / G^1(0) \quad (21)$$

Numerical computation of $a_n(X)$, $g_1(X)$ and $g_2(X)$ is again so easy (see appendices A and B) that numerical results are shown graphically for a later comparison; $a_n(X)$ in fig. 4, and $g_1(X)$ and $g_2(X)$ in fig. 5.

2.3. Remarks

In the case of long rods, we have $D_3 - D_1 > 0$ and hence $\mu^2 > 0$. For $\mu^2 \gg 1$ or $k \gg 1$, the operator $-\nabla_\xi^2 + \mu^2 \xi^2$ in eq. 2 can be reduced to that of a harmonic oscillator and we can know analytically the limiting values of $f_1(k) \to 1$ and $f_2(k) \to 0$ as $k \to \infty$ [6]. In the case of large discs, on the other hand, we have $D_3 - D_1 < 0$ and hence $\mu^2 < 0$. In this case, we have no simple way to estimate analytically the limiting values of $g_1(X)$ and $g_2(X)$ at large X. We numerically computed both functions for very large X values (fig. 5) and found that $g_1(X) \to 2$ and $g_2(X) \to 1$ as $X \to \infty$.

For a rigid rod with $\mu = 0$ or $D_3 = D_1$, $\boldsymbol{M}$ in eq. 3 is diagonal and we have $\lambda_l = l(l+1)$ and $\boldsymbol{U} = \boldsymbol{U}^{-1} = \boldsymbol{E}$ (the unit matrix). Then, we have $[\boldsymbol{U} \exp(-\Theta \boldsymbol{\Lambda} \tau) \boldsymbol{U}^{-1}]_{nl} = \exp[-n(n+1)\Theta\tau]\delta_{nl}$ and, from eq. 6,

$$G^1(\tau) = \sum_n S_n(k) \exp\left[-\left\{ D_0 K^2 + n(n+1)\Theta \right\} \tau \right] \quad (22)$$

where $S_n(k) = (2n+1) b_n(k)^2$. This is just the Pecora result [2] as we have discussed [6,8]. The time derivative of eq. 22 gives eq. 14 for $D_3 = D_1$, where $f_2(k)$ does not appear because of the absence of off-diagonal elements in $\boldsymbol{M}$. Recent careful experiments on monodisperse suspensions of tobacco mosaic virus, however, clearly indicated a quantitative importance of anisotropy in translational diffusion [8,17].

The $G^1(\tau)$ for a rigid disc with $D_3 = D_1$ is also given by eq. 22, provided that $S_n(k)$ for a rod is replaced with $H_n(X) = (2n+1) a_n(X)^2$ for a disc. Numerical values of our $(2n+1) a_n(X)^2$ agree with those of analytical expressions for $H_n(X)$ (we thank one of the reviewers who kindly sent us his unpublished results on $H_n(X)$). In this case again, $g_2(X)$ does not appear in eq. 19. Similarly to the case of tobacco mosaic virus, however, large effects of anisotropy in translational diffusion on $\bar{\Gamma}/K^2$ values and profiles of $G^1(\tau)$ will surely be detected for monodisperse preparations of rigid discs with favorable dimensions.

3. Discussion

Since $f_1(0) = g_1(0) = 0$ and $f_2(0) = g_2(0) = 1/3$, we have

$$\bar{\Gamma}/K^2 \to D_0 \qquad (k \ll 1 \text{ or } X \ll 1)$$

In either case, suspensions of rigid rods or rigid discs, we can determine the overall translational diffusion coefficient D_0 from low-angle data of $\bar{\Gamma}$. Once we know D_0 of the rod, the least-squares analysis by use of eq. 14 provides the values of Θ and $(D_3 - D_1)$. Thus, we can obtain transport coefficients D_1, D_3 and Θ of a rigid rod from light-scattering data only, as has been shown for tobacco mosaic virus [8]. Similarly, we will obtain D_1, D_3 and Θ of a rigid disc by use of eq. 19, provided that the situation is favorable.

Since $f_1(\infty) = 1$ and $f_2(\infty) = 0$, we have

$$\bar{\Gamma}/K^2 \to D_1 + (L^2/12)\Theta \qquad (k \gg 1)$$

In the long-rod limit, neglect of the end effect gives $\Theta = 12D_1/L^2$, so that we have $\bar{\Gamma}/K^2 \to D_1 + D_1$ at $k \gg 1$. From eq. 13 we have

$$G^1(0) = \sum_n (2n+1)c_n(0, k)^2 = \tfrac{1}{2}\int_{-1}^{1} j_0(k\xi)^2 \, d\xi$$

where use was made of $\delta(\xi - \xi') = \Sigma_n[(2n+1)/2]P_n(\xi)P_n(\xi')$. For large k values, the intensity $G^1(0)$ is exclusively contributed from rods with orientation $\xi = 0$ (or perpendicular to $\boldsymbol{K}$) because of a sharp peak of $j_0(k\xi)$ at $\xi = 0$. This is the reason why only $D_1 + D_1$ can be observed at $k \gg 1$ [6].

Since $g_1(\infty) = 2$ and $g_2(\infty) = 1$, on the other hand, we have

$$\bar{\Gamma}/K^2 \to D_3 + (R^2/4)2\Theta \qquad (X \gg 1)$$

Perrins's formulas give $\Theta = (3/2)D_3/R^2$ for $R \gg a$ (the half-thickness of a disc) [11], so that $\bar{\Gamma}/K^2 \to D_3 + (3/4)D_3$. Similarly to the case of rods, we have from eq. 17

$$G^1(0) = \sum_n (2n+1)c_n(X, 0)^2 = \tfrac{1}{2}\int_{-1}^{1} [2J_1(Y)/Y]^2 d\xi$$

For large X values, the intensity $G^1(0)$ is exclusively contributed from discs with orientation $\xi = \pm 1$ (or the normal to the disc plane is parallel with $\boldsymbol{K}$) because of sharp peaks of $[2J_1(Y)/Y]^2$ at $\xi = \pm 1$. This is the reason why only $D_3 + (3/4)D_3$ can be observed at $X \gg 1$.

In an intermediate range of k values, $\bar{\Gamma}/K^2$ values of rods increase almost monotonically as k increases (fig. 9 given later), although $f_2(k)$ has a slight shoulder at around $k = 5$ (fig. 3). On the other hand, $\bar{\Gamma}/K^2$ values of discs show distinct anomaly as shown in fig. 10 (given later). This arises from fluctuating increases of $g_1(X)$ and $g_2(X)$ as shown in fig. 5. The most dominant contribution to these fluctuating increases is from anomalous behavior of $a_0(X)$, i.e., $a_0(X) = 0$ at $X = 2\pi m$.

Since extremely prolate and oblate ellipsoids of revolution correspond to a rod and a disc, respectively, we considered the light-scattering problem for an ellipsoidal and an ellipsoid shell of revolution in appendix C.

4. Concluding remarks

If the experimental $\bar{\Gamma}/K^2$ values exceed those predicted by eq. 14 for reasonable values of D_1, D_3 and Θ, we have to take account of a possible contribution to $\bar{\Gamma}/K^2$ from flexing motions of long rods, as has been discussed for fd virus ($L = 895$ nm and $2R = 9$ nm) [12–14]. Similarly, if

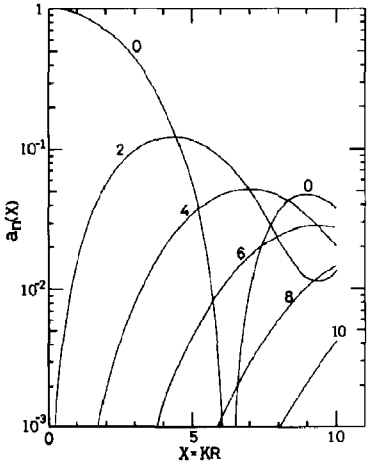

Fig. 4. Graphic representation of the dynamic form factors $a_n(X)$ for a rigid disc with radius R.

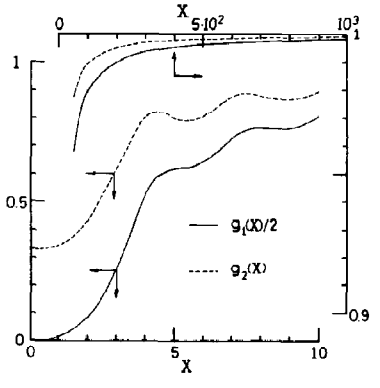

Fig. 5. Graphic representation of the functions $g_1(X)$ and $g_2(X)$ for a rigid disc. Note that both functions increase oscillatorily as X increases.

experimental $\bar{\Gamma}/K^2$ values exceed those expected from eq. 19 for reasonable values of D_1, D_3 and Θ, we have to take account of a possible contribution to $\bar{\Gamma}/K^2$ from bending motions of discs. A theoretical model of the effect of bending motions of discs on $G^1(\tau)$ will be discussed elsewhere.

An application of the present formulation to the analysis of experimental data is discussed in the accompanying paper [7].

Appendix A: Alternate expressions for the dynamic form factors for thin rods and thin discs

To give a little generality to our result, we first start here from a hollow cylinder whose outer and inner radii are R and r, respectively. Apart from a factor $\exp[i\boldsymbol{K}\cdot\boldsymbol{R}(t)]$, we have

$$a(K,\theta,t)=\frac{2}{R^2-r^2}\int_r^R J_0(K\rho\sin\theta)\rho\,\mathrm{d}\rho \times\frac{1}{L}\int_{-L/2}^{L/2}e^{iKz\xi}\,\mathrm{d}z \tag{A1}$$

$$=\frac{1}{R^2-r^2}\left[R^2(2J_1(Y)/Y) -r^2(2J_1(y)/y)\right]j_0(k\xi) \tag{A2}$$

where $Y=KR\sin\theta=X\sin\theta$ and $y=Kr\sin\theta=x\sin\theta$. By multiplying both sides of eq. A2 by $\frac{1}{2}P_n(\xi)$ which comes from $g_K(\xi,\xi';\tau)$, and integrating over ξ, we have the dynamic form factors $c_n(X,x,k)$ for the hollow cylinder as

$$c_n(X,x,k)=\frac{1}{R^2-r^2}\left[R^2c_n(X,k)-r^2c_n(x,k)\right] \tag{A3}$$

where $c_n(X,k)$ is given by eq. 7. For $k\ll 1$, we obtain the dynamic form factors $a_n(X,x)$ for a ring as

$$a_n(X,x)\equiv c_n(X,x,0) =\frac{1}{R^2-r^2}\left[R^2a_n(X)-r^2a_n(x)\right] \tag{A4}$$

where $a_n(X)$ is given by eq. 17 or eq. A9 given below.

By use of the formulas [9,10]

$$J_0(z\sin\theta)=\sum_{m=0}^{\infty}(4m+1)f(m)j_{2m}(z)P_{2m}(\xi) \tag{A5}$$

$$\exp(iz\xi)=\sum_{q=0}^{\infty}(2q+1)(i)^q j_q(z)P_q(\xi) \tag{A6}$$

where $f(m)=(2m-1)!!/(2^m m!)$, we have from eq. A1

$$c_n(X,x,k)=\sum_{m=0}^{\infty}\sum_{q=0}^{\infty}(4m+1)(4q+1) \times a_{2m}(X,x)(-1)^q b_{2q}(k) \times P(2m,2q,n) \tag{A7}$$

where $a_{2m}(X,x)$ is given by eq. A4 and

$$b_{2q}(k)=(1/k)\int_0^k j_{2q}(z)\mathrm{d}z \tag{A8}$$

$$a_{2m}(X)=f(m)(2/X^2)\int_0^X j_{2m}(z)z\,\mathrm{d}z \tag{A9}$$

$$P(2m,2q,n) =(1/2)\int_{-1}^{1}P_{2m}(\xi)P_{2q}(\xi)P_n(\xi)\mathrm{d}\xi \tag{A10}$$

Eqs. A7, A8 and A9 are alternate expressions of eqs. A3, 13 and 17, respectively. $P(2m,2q,n)\neq 0$ for even n will be given by Wigner's $3j$ symbols [15].

For a thin hollow cylinder (i.e., $X-x\ll 1$ or $R\simeq r$), the integration over ρ in eq. A1 gives $J_0(X^*\sin\theta)$ with $X^*=KR^*$ and $R^*=(R+r)/2$. Then, we have the dynamic form factors $c_n^*(X^*,k)$ for the thin hollow cylinder as

$$c_n^*(X,k)=\sum_{m=0}^{\infty}\sum_{q=0}^{\infty}(4m+1)(4q+1)(-1)^q \times a_{2m}^*(X^*)b_{2q}(k)P(2m,2q,n) \tag{A11}$$

where

$$a_{2m}^*(X^*)=f(m)j_{2m}(X^*) \tag{A12}$$

Eq. A12 gives the dynamic form factors for a thin ring.

Appendix B: Numerical computation of $a_{2m}(X)$ and $b_{2m}(k)$

The direct evaluation of eq. 17 or eq. A9 for $a_{2m}(X)$ (or eq. 13 or eq. A8 for $b_{2m}(k)$) is not difficult. However, the following methods are more appropriate for numerical computation of $a_{2m}(X)$ and $b_{2m}(k)$. By use of an integral formula for the Bessel function ($\mathrm{Re}(\mu+\nu+1)>0$) [10]

$$\int_0^z t^{\mu} J_{\nu}(t)\mathrm{d}t = z^{\mu}\frac{\Gamma\left(\frac{\nu+\mu+1}{2}\right)}{\Gamma\left(\frac{\nu-\mu+1}{2}\right)} \times \sum_{l=0}^{\infty}(\nu+2l+1)\frac{\Gamma\left(\frac{\nu-\mu+1}{2}+l\right)}{\Gamma\left(\frac{\nu+\mu+3}{2}+l\right)} \times J_{\nu+2l+1}(z) \qquad \text{(B1)}$$

we have from eqs. A8 and A9

$$b_{2m}(k) = (2/k)\sum_{l=m}^{\infty}\frac{l+\frac{3}{4}}{l+\frac{1}{2}}\cdot\frac{f(m)}{f(l)}j_{2l+1}(k) \qquad \text{(B2)}$$

$$a_{2m}(X) = (4/X)\sum_{l=m}^{\infty}\frac{l+\frac{3}{4}}{l+1}\cdot f(l)\,j_{2l+1}(X) \qquad \text{(B3)}$$

where use was made of $j_n(z) = (\pi/2z)^{1/2} \times J_{n+1/2}(z)$. Without numerical integration, eqs. B2 and B3 give $b_n(k)$ and $a_n(X)$, respectively. This is important for their evaluation for very large values of k and X, respectively. The integration (or summation) over the argument z of $j_{2m}(z)$ is required in eqs. A8 and A9, whereas the summation over the order l of $j_{2l+1}(z)$ is required in eqs. B2 and B3. To sum over order is much easier than to sum over argument; no special examination about the convergence of the result is required in the former because of the integral nature of l. It should be noted that the recurrence relation $j_{n-1}(z) = [(2n+1)/z]j_n(z) - j_{n+1}(z)$ (and $J_{n-1}(z) = (2n/z)J_n(z) - J_{n+1}(z)$ which will be used in appendix C) is stable for decreasing n [10]. Although $f(m)$ is a slowly decreasing function of m and $|j_{2m+1}(z)| < 0.5$ for $m \geqslant 1$ and $z \geqslant 0$, the convergence of the summation over l is not poor, because $|j_{2m+1}(z)|$ becomes very small above a certain number of m. At $X = 50$, for example, we know $10^{-5} < |j_{2m+1}(X)| < 10^{-2}$ for $m \leqslant 30$ and $|j_{2m+1}(X)| < 10^{-28}$ for $m > 55$.

A brief description of an algorithm for the evaluation of $b_{2m}(k)$ and $a_{2m}(X)$ is given below. Assume that an array AM(0:150) has been reserved. Our program for $0.1 \leqslant X$ (or k) $\leqslant 50$ runs in the following steps:

(1) Give an X (or k) value,

(2) set $N = 30$, $N_m = 40$ and $M = 14$ for $0.1 \leqslant X$ (or k) $\leqslant 1.5$, or $N = 2X + 40$, $N_m = N + 40$ and $M = (X + 30)/2$ for $1.5 < X$ (or k) $\leqslant 50$,

(3) starting from $j_{N_m+1}(X) = 0$ and $j_{N_m}(X) = 1.0 \times 10^{-75}$, compute $j_n(X)$ for $N \geqslant n \geqslant 0$ and store the normalized $j_n(X)$ on AM(n) for each n (where the normalization of $j_n(X)$ was made by referring $j_0(X) = (\sin X)/X$ or $j_1(X) = (\sin X - X\cos X)/X^2$; the normalization of $J_n(X)$ used in appendix C was made by a relationship $J_0(X) + 2\Sigma'_n J_{2n}(X) = 1$),

(4) compute $f(m)$ for $0 \leqslant m \leqslant N/2$ and store $f(m)$ on AM($2m$) for each m,

(5) compute eq. B3 (or B2) for $0 \leqslant m \leqslant M$ (in the direction of increasing m) and $m \leqslant l \leqslant (N/2 - 1 - m)$, and store $a_{2m}(X)$ (or $b_{2m}(k)$) on AM($2m$) for each m,

(6) compute $G^1(0)$, $g_1(X)$ and $g_2(X)$ (or $f_1(k)$ and $f_2(k)$),

(7) type out required results,

(8) return to (1) for the next X (or k) value, otherwise stop.

Our program was tested by comparing $G^1(0) = \Sigma_m(4m+1)a_{2m}(X)^2$ with $P(X) = (2/X^2)(1 - J_1(2X)/X)$, and it was found that $|G^1(0) - P(X)|/G^1(0) \leqslant 10^{-8}$. The program in FORTRAN took 3 s for $X = 50$ with a minicomputer (Nippon Data General, Nova 02/30), and in BASIC, 20 s for $X = 5$ and 120 s for $X = 50$ with a desk-top microcomputer (Hewlett-Packard, HP-85). For a practical range of X (or k), any desk-top computer can work with a reasonable computation time. [For very large X (or k) values, we set $N = 2X + 90$, $N_m = N + 0.05X + 40$ and $M = (X + 40)/2$. In this case, over- and under-flow problems must be considered at step (3). Our minicomputer took 280 s for $X = 1000$ (see fig. 5); most of the time was required at step (5).]

Appendix C: Alternate models

For an ellipsoid of revolution

$$x^2/b^2 + y^2/b^2 + z^2/a^2 = r^2 \tag{C1}$$

with $r = 1$, we have (apart from the factor $\exp[i\boldsymbol{K}\cdot\boldsymbol{R}(t)]$)

$$a(K, \theta, t) = \frac{1}{(4\pi ab^2/3)} \iiint \mathrm{d}x\, \mathrm{d}y\, \mathrm{d}z \times \exp[iK(-x \sin\theta \cos\Phi + y \sin\theta \sin\Phi + z \cos\theta)] \tag{C2}$$

The integration in eq. C2 can be carried out by the method of Norisuye and Yu [16]. Letting $x = ub$, $y = vb$ and $z = wa$, we have

$$a(K, \theta, t) = (3/4\pi) \iiint_{u^2+v^2+w^2\le 1} \mathrm{d}u\, \mathrm{d}v\, \mathrm{d}w \times \exp[iKb(-u \sin\theta \cos\Phi + v \sin\theta \sin\Phi + p^{-1} w \cos\theta)] \tag{C3}$$

where $p = b/a$ is the axial ratio ($p > 1$ for oblate and $0 < p < 1$ for prolate). Let (ρ, α, β) be the polar coordinates of (u, v, w), i.e., $u = \rho \sin\beta \cos\alpha$, $v = \rho \sin\beta \sin\alpha$ and $w = \rho \cos\beta$. By use of Poisson's formula [9]

$$\int_0^{\pi} \mathrm{d}\beta \int_0^{2\pi} f(a \cos\beta + b \sin\beta \cos\alpha + c \sin\beta \sin\alpha) \sin\beta\, \mathrm{d}\alpha = 2\pi \int_{-1}^{1} f\left[(a^2+b^2+c^2)^{1/2} s\right] \mathrm{d}s$$

we have from eq. C3

$$a(K, \theta, t) = \tfrac{3}{2} \int_0^1 \rho^2 \mathrm{d}\rho \int_{-1}^{1} \exp(iZ\rho s)\, \mathrm{d}s \tag{C4}$$

$$= 3 \int_0^1 j_0(Z\rho) \rho^2 \mathrm{d}\rho \tag{C4'}$$

$$= 3 j_1(Z)/Z \tag{C4''}$$

where $q = 1 - p^{-2}$, $\xi = \cos\theta$ and

$$Z = Kb(1 - q\xi^2)^{1/2} \tag{C5}$$

$$\to Kb \sin\theta \qquad (p \gg 1) \tag{C5'}$$

$$\to Ka \cos\theta \qquad (0 < p \ll 1) \tag{C5''}$$

The dynamic form factors $d_n(K, a, b)$ for the ellipsoid of revolution will be given by

$$d_n(K, a, b) = \int_0^1 [3j_1(Z)/Z]\, P_n(\xi)\mathrm{d}\xi \quad (\text{even } n); \qquad = 0 \quad (\text{odd } n) \tag{C6}$$

For limiting ellipsoids, more appropriate expressions than eq. C6 for numerical computation of $d_n(Kb) \equiv d_n(K, a \ll b)$ and $d_n(Ka) \equiv d_n(K, a \gg b)$ can be derived as follows: By use of the formulas [9,10]

$$\sin(z \sin\theta) = 2 \sum_{l=0}^{\infty} J_{2l+1}(z) \sin[(2l+1)\theta] \tag{C7}$$

$$\tfrac{1}{2} \int_0^{\pi} \sin[(2l+1)\theta]\, P_{2m}(\cos\theta)\mathrm{d}\theta = \frac{1}{2l+2m+1} \cdot \frac{f(l-m)}{f(l+m)} \quad (l \ge m); \qquad = 0 \quad (l < m) \tag{C8}$$

and eq. B1, we have from eqs. C4' and C5'

$$d_{2m}(Kb) = \left[6/(Kb)^2\right] \sum_{l=m}^{\infty} \frac{l+\frac{1}{2}}{l+m+\frac{1}{2}} \cdot \frac{f(l-m)}{f(l+m)} \times \sum_{q=l}^{\infty} \frac{q+1}{(q+\frac{3}{2})(q+\frac{1}{2})} J_{2q+2}(Kb) \qquad (p \gg 1) \tag{C9}$$

By use of eqs. A6 and B1, we have from eqs. C4 and C5''

$$d_{2m}(Ka) = (-1)^m \left[12/(Ka)^2\right] f(m) \sum_{l=m}^{\infty} (l+\tfrac{3}{4}) \times \sum_{q=l}^{\infty} \frac{q+\frac{5}{4}}{(q+\frac{3}{2})(q+\frac{1}{2})} \cdot \frac{1}{f(q)} j_{2q+2}(Ka) \qquad (0 < p \ll 1) \tag{C10}$$

For an ellipsoidal shell, the integration $(3/4\pi)\iiint f(\rho, \alpha, \beta)\rho^2 \sin\beta\, \mathrm{d}\rho\, \mathrm{d}\alpha\, \mathrm{d}\beta$ in eq. C3 should be replaced by $(1/4\pi)\iiint f(1, \alpha, \beta)\sin\beta\, \mathrm{d}\alpha\, \mathrm{d}\beta$ and we have

$$a(K, \theta, t) = j_0(Z) \tag{C11}$$

which has been derived by Norisuye and Yu [16]. The dynamic form factors $d_n^s(K, a, b)$ for the ellipsoidal shell will be given by

$$d_n^s(K, a, b) = \int_0^1 j_0(Z) P_n(\xi) \mathrm{d}\xi \quad \text{(even } n\text{)}$$
$$= 0 \quad \text{(odd } n\text{)} \tag{C12}$$

By use of eqs. C7 and C8, we have from eqs. C12 and C5′

$$d_{2m}^s(Kb) = [1/(Kb)] \sum_{l=m}^{\infty} \frac{1}{l+m+\frac{1}{2}} \times \frac{f(l-m)}{f(l+m)} J_{2l+1}(Kb) \quad (p \gg 1) \tag{C13}$$

From eq. C11 and C5″, we have

$$d_{2m}^s(Ka) = (-1)^m b_{2m}(Ka) \quad (0 < p \ll 1) \tag{C14}$$

where $b_{2m}(z)$ is given by eq. B2.

The radius of gyration of the ellipsoid given by eq. C1 with $r = 1$ around its x-axis is given by $(a^2 + b^2)/5$. Let us define an ellipsoidal shell by two ellipsoids, eq. C1 with $r = 1$ and $r < 1$. Let

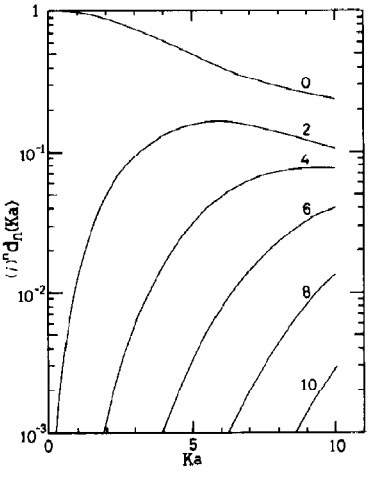

Fig. 6. Graphic representation of the dynamic form factors $(i)^n d_n(Ka)$ for an extremely prolate ellipsoid of revolution with the major radius a. This figure should be compared with fig. 2.

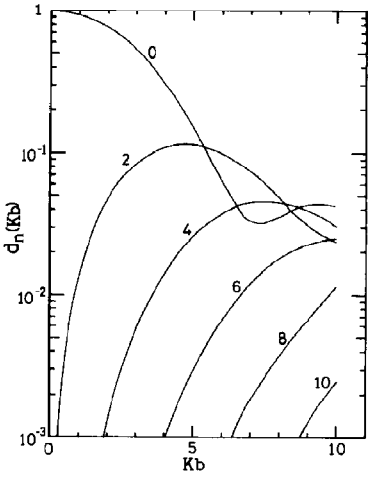

Fig. 7. Graphic representation of the dynamic form factors $d_n(Kb)$ for an extremely oblate ellipsoid of revolution with the major radius b. This figure should be compared with fig. 4.

$m = 4\pi ab^2/3$ and $m_r = mr^3$. Then, the radius of gyration of the shell around its x-axis is given by $\langle R_g^2 \rangle = [m\langle R_g^2 \rangle_1 - m_r \langle R_g^2 \rangle_r]/(m - m_r) \to (a^2 + b^2)/3$ as $r \to 1$. We have $\langle R_g^2 \rangle = b^2/5$ for oblate $(p \gg 1)$ and $a^2/5$ for prolate $(0 < p \ll 1)$ ellipsoids of revolution, and $\langle R_g^2 \rangle = b^2/3$ for oblate and $a^2/3$ for prolate ellipsoidal shells.

Extremely oblate and prolate ellipsoids of revolution correspond to a disc and a rod, respectively. The dynamic form factors $d_{2m}(Kb)$ in eq. C9, $d_{2m}(Ka)$ in eq. C10 and $d_{2m}^s(Kb)$ in eq. C13 can easily be computed according to the algorithm given in appendix B with very slight modifications. Therefore, we give results graphically in figs. 6–10 for comparative purpose only.

Since $3j_1(z)/z = j_0(z) + j_2(z)$, we have the following relationship

$$d_{2m}(K, a, b) = d_{2m}^s(K, a, b) + \int_0^1 j_2(Z) P_{2m}(\xi) \mathrm{d}\xi$$

By use of an integral representation of the Neumann function $N_n(z)$ (or the Bessel function of the second kind) [9], we have for $Kb > 0$

$$d_0^s(Kb) = [\pi/(2Kb)] N_0(Kb) + S(Kb)$$

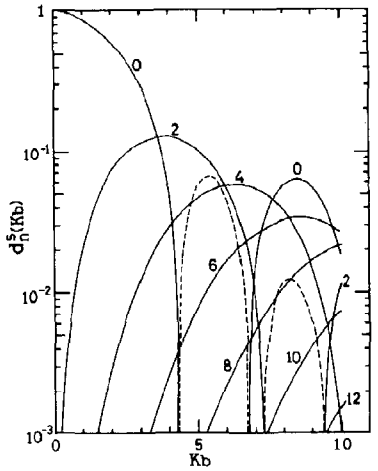

Fig. 8. Graphic representation of the dynamic form factors $d_n^s(Kb)$ for an extremely oblate ellipsoidal shell of revolution with the major radius b. The dashed parts have the negative sign. This figure should also be compared with fig. 4.

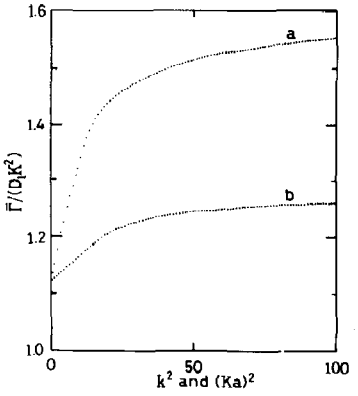

Fig. 9. Graphic representation of the $\bar{\Gamma}/(D_1K^2)$ vs. K^2 relationship for a rod-like scatterer. Parameter values were $D_1 = 3.61\times10^{-8}$ cm^2/s, $D_3 = 5.64\times10^{-8}$ cm^2/s, $\Theta = 312$ s^{-1} and $L = 300$ nm (those for tobacco mosaic virus [8]). Curve a for a rod ($\langle R_g^2\rangle = L^2/12$) and for an extremely prolate ellipsoidal shell of revolution ($\langle R_g^2\rangle = a^2/3$ with $2a = L$); curve b for an extremely prolate ellipsoid of revolution ($\langle R_g^2\rangle = a^2/5$ with $2a = L$).

where

$$S(Kb) = [1/(Kb)]\int_0^\infty \exp(-Kb\sinh t)\,dt$$

Since $S(Kb) > 0$ and $\partial S(Kb)/\partial(Kb) < 0$, $S(Kb)$ is a rapidly and monotonically decreasing function of Kb. Zero points of $d_0^s(Kb)$ are thus close to those of $N_0(Kb)$ except for the first zero point of the latter. Contrary to $a_0(X)$ for a disc, $d_0^s(Kb)$ changes its sign in nearly the same way as $N_0(Kb)$ does. As shown in fig. 8, $d_0^s(Kb)$ and $d_2^s(Kb)$ change their sign in the range $0 \leqslant Kb \leqslant 10$. Mainly due to these types of behavior, $g_1(Kb)$ and $g_2(Kb)$ show much stronger fluctuating increases than those of $g_1(X)$ and $g_2(X)$ in fig. 5. On the other hand, $d_0(Kb)$ is positive and shows the first minimum at $Kb \simeq 7.5$. Mainly due to this behavior, $g_1(Kb)$ and $g_2(Kb)$ for the extremely oblate ellipsoid show slightly fluctuating increases. Quite a variety in the K dependence of form factors for different models arises solely from differences in distribution of the scattering mass. We briefly discuss this point.

First, we consider $b_{2m}(k)$, $d_{2m}(Ka)$ and $d_{2m}^s(Ka)$. For an ellipsoid defined by eq. C1 with $r = 1$, the mass density at z is given by $m(z) = \pi x^2(=\pi y^2) = \pi b^2[1-(z/a)^2]$. The integration of $m(z)$ over z from $-a$ to a gives the total mass $m = 4\pi ab^2/3$ of the ellipsoid. The normalized distribution, $\bar{m}(z) = m(z)/m = (3/4a)[1-(z/a)^2]$ with $(3/4a) = 1$, is plotted in fig. 11a. If we assume $Kb \ll 1$ (i.e., an extremely prolate ellipsoid), we have

$$a(K,\xi,t) = (1/m)\int_{-a}^{a} m(z)\exp(iKz\xi)\,dz$$
$$= 3j_1(u)/u$$

where $u = Ka\xi$. This equation is the same as eq. C4'' with eq. C5''. For an ellipsoidal shell defined by two ellipsoids with $r = 1$ and $r < 1$, we have $m_1(z) = \pi b^2[1-(z/a)^2]$ and $m_r(z) = \pi b^2 r^2[1-(z/ar)^2]$. The total mass of the shell is given by $m^s = m_1 - m_r = (4\pi ab^2/3)(1-r^3)$. For $Kb \ll 1$, we have

$$a(K,\xi,t) = (1/m^s)\left[\int_{-a}^{a} m_1(z)\exp(iKz\xi)\,dz - \int_{-ar}^{ar} m_r(z)\exp(iKz\xi)\,dz\right]$$
$$= \left[3j_1(u)/u - r^3\{3j_1(ur)/(ur)\}\right]/(1-r^3)$$

By putting $r = 1-\delta$ ($\delta \simeq 0$) and by use of $dj_1(z)/dz = j_0(z) - 2j_1(z)/z$, we finally obtain for $\delta \to 0$ or $r \to 1$

$$a(K,\xi,t) = j_0(u)$$

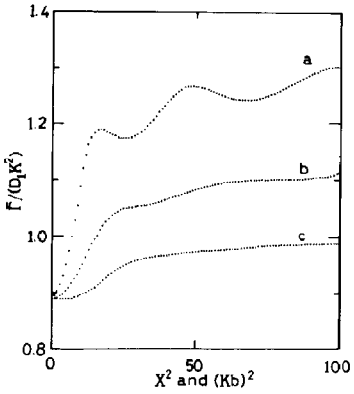

Fig. 10. Graphic representation of the $\bar{\Gamma}/(D_1K^2)$ vs. K^2 relationship for a disc-like scatterer. Parameter values were $D_1 = 1.458\times10^{-8}$ cm²/s, $D_3 = 0.979\times10^{-8}$ cm²/s, $\Theta = 16.9$ s^{-1} and $R = 295$ nm. Curve a for an extremely oblate ellipsoidal shell of revolution ($\langle R_g^2\rangle = b^2/3$ with $b = R$); curve b for a disc ($\langle R_g^2\rangle = R^2/4$); curve c for an extremely oblate ellipsoid of revolution ($\langle R_g^2\rangle = b^2/5$ with $b = R$).

which is the same as eq. C11 with eq. C5″. The normalized distribution, $\bar{m}^s(z) = [m_1(z) - m_r(z)]/m^s$ with $(3/4a) = 1$, is plotted in fig. 11a. In the limit of $r \to 1$, $\bar{m}^s(z)$ is flat like a rod. Next, we consider $a_{2m}(X)$, $d_{2m}(Kb)$ and $d^s_{2m}(Kb)$. The thickness of an oblate ellipsoid at a point (x, y) is given by $2z$. Thus, the mass density (integrated over z) is given by $m(\rho) = 2a[1-(\rho/b)^2]^{1/2}$, where $x = \rho\cos\phi$ and $y = \rho\sin\phi$. The total mass is given by $m = 2\pi\int m(\rho)\rho\,d\rho = (4\pi ab^2/3)$. The normalized distribution, $\bar{m}(\rho) = m(\rho)/m = (3/2\pi b^2)[1-(\rho/b)^2]^{1/2}$ with $(3/2\pi b^2) = 1$, is plotted in fig. 11b. For $Ka \ll 1$ (or an extremely oblate ellipsoid of revolution) we have

$$a(K,\theta,t) = (2\pi/m)\int_0^b m(\rho)J_0(K\rho\sin\theta)\rho\,d\rho$$
$$= 3\int_0^{\pi/2} J_0(v\sin\alpha)\cos^2\alpha\sin\alpha\,d\alpha$$

where $v = Kb\sin\theta$ and $\sin\alpha = \rho/b$. By use of the formula [9,10]

$$\int_0^{\pi/2} J_\nu(v\sin\alpha)\cos^{2\lambda+1}\alpha\sin^{\nu+1}\alpha\,d\alpha$$
$$= 2^\lambda v^{-\lambda-1}\Gamma(\lambda+1)J_{\lambda+\nu+1}(v)$$
$$(\mathrm{Re}\,\nu,\ \mathrm{Re}\,\lambda > -1)$$

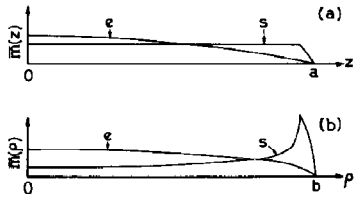

Fig. 11. The normalized mass distribution (see text). (a) Mass distribution for extremely prolate ellipsoid e and ellipsoidal shell s of revolution along the z-axis; and (b) mass distribution for extremely oblate ellipsoid e and ellipsoidal shell s of revolution along the radial direction. Curves for shells were drawn for $r = 1$ and $r = 0.95$.

we have

$$a(K,\theta,t) = 3j_1(v)/v$$

The mass densities (integrated over z) at a point (x, y) of ellipsoids of revolution with $r = 1$ and $r < 1$ are given by $m_1(\rho) = 2a[1-(\rho/b)^2]^{1/2}$ and $m_r(\rho) = 2ar[1-(\rho/br)^2]^{1/2}$, respectively. The total mass of the ellipsoidal shell is given by $m^s = (4\pi ab^2/3)(1-r^3)$. For $Ka \ll 1$, we have

$$a(K,\theta,t) = (2\pi/m^s)\left[\int_0^b m_1(\rho)J_0(K\rho\sin\theta)\rho\,d\rho - \int_0^{br} m_r(\rho)J_0(K\rho\sin\theta)\rho\,d\rho\right]$$
$$= \left[3j_1(v)/v - r^3\{3j_1(vr)/(vr)\}\right]/(1-r^3)$$

In the limit of $r \to 1$, therefore, we have

$$a(K,\theta,t) = j_0(v)$$

The normalized distribution, $\bar{m}^s(\rho) = [m_1(\rho) - m_r(\rho)]/m^s$ with $(3/2\pi b^2) = 1$, is plotted in fig. 11b.

As discussed above, differences in mass distribution give quite a different K dependence of dynamic form factors as well as the values of radii of gyration.

Acknowledgement

We thank Miss Michiho Takasaki for her assistance in machine computation.

References

1 B. Chu, Laser light scattering (Academic Press, New York, 1974).
2 B. Berne and R. Pecora, Dynamic light scattering (Interscience, New York, 1975).
3 S.-H. Chen, B. Chu and R. Nossal, Scattering techniques applied to supramolecular and nonequilibrium system (Plenum Press, New York, 1981).
4 D.B. Sattelle, W.I. Lee and B.R. Ware, Biomedical application of laser light scattering (Elsevier Biomedical Press, Amsterdam, Oxford, 1982).
5 J.C. Earnshaw and M.W. Steer, The application of laser light scattering to the study of biological motion (Plenum Press, New York, 1983).
6 T. Maeda and S. Fujime, Macromolecules 17 (1984) 1157.
7 K. Kubota, Y. Tominaga, S. Fujime, J. Otomo and A. Ikegami, Biophys. Chem. 23 (1985) 15.
8 K. Kubota, H. Urabe, Y. Tominaga and S. Fujime, Macromolecules 17 (1984) 2096.
9 S. Moriguchi, K. Udagawa and S. Hitotsumatsu, Mathematical formulas I, II and III (Iwanami, Tokyo, 1959).
10 M. Abramowitz and I.A. Stegun, Handbook of mathematical functions with formulas, graphs and mathematical tables, 9th edn. (Dover Publications, New York, 1970).
11 F. Perrin, J. Phys. Radium 5 (1934) 497.
12 T. Maeda and S. Fujime, Macromolecules 17 (1984) 2381.
13 S. Fujime and T. Maeda, Macromolecules 18 (1985) 191.
14 T. Maeda and S. Fujime, Macromolecules (1985) in the press.
15 A. Messiah, Quantum mechanics, vol. II (Wieley, New York, 1962).
16 T. Norisuye and H. Yu, Biochim. Biophys. Acta 471 (1977) 436.
17 J. Wilcoxon and J.M. Schurr, Biopolymers 22 (1983) 849.